^{64}Cu-Labeled Repebody Molecules for Imaging of Epidermal Growth Factor Receptor–Expressing Tumors

Ayoung Pyo*[1,2], Misun Yun*[1,3], Hyeon Sik Kim[1], Tae-Yoon Kim[4], Joong-jae Lee[4], Jung Young Kim[5], Sunwoo Lee[2], Seong Young Kwon[1], Hee-Seung Bom[1], Hak-Sung Kim[4], Dong-Yeon Kim[1], and Jung-Joon Min[1]

[1]Department of Nuclear Medicine, Chonnam National University Hwasun Hospital, Hwasun, Korea; [2]Department of Chemistry, Chonnam National University, Gwangju, Korea; [3]Chair for Biological Imaging, Technische Universitat München, Munich, Germany; [4]Department of Biological Sciences, Korea Advanced Institute of Science and Technology (KAIST), Daejeon, Korea; and [5]Division of RI-Convergence Research, Korea Institute of Radiological and Medical Sciences, Seoul, Korea

The epidermal growth factor receptor (EGFR) is a member of the erbB family of receptors and is overexpressed in many tumor types. A repebody is a newly designed nonantibody protein scaffold for tumor targeting that contains leucine-rich repeat modules. In this study, 3 ^{64}Cu-labeled anti-EGFR repebodies with different chelators were synthesized, and their biologic characteristics were assessed in cultured cells and tumor-bearing mice. **Methods:** Repebodies were synthesized with the chelators 2-(*p*-isothiocyanatobenzyl)-1,4,7-triazacyclononane-*N,N′,N,″*-triacetic acid trihydrochloride ([*p*-SCN-Bn]-NOTA), 2,2′,2″-(10-(2-(2,5-dioxopyrrolidin-1-yloxy)-2-oxoethyl)-1,4,7,10-tetraazacyclododecane-1,4,7-triyl) triacetic acid (DOTA-*N*-hydroxysuccinimide ester), or 1-(*p*-isothiocyanatobenzyl) diethylenetriamine pentaacetic acid trihydrochloride ([*p*-SCN-Bn]-DTPA) in 1.0 M $NaHCO_3$ buffer (pH 9.2) for 24 h. Purified NOTA-, DOTA-, and DTPA-conjugated repebody were radiolabeled with ^{64}Cu in 0.1 M NH_4OAc buffer (pH 5.5). To compare the EGFR-binding affinities of the repebodies, cellular uptake studies were performed with the human non–small cell lung cancer cell line H1650 (high expression of EGFR) and the human colon adenocarcinoma cell line SW620 (low expression of EGFR). Biodistribution and small-animal PET imaging studies were performed using H1650 tumor–bearing mice. **Results:** Radiochemical yields of the ^{64}Cu-labeled repebodies were approximately 70%–80%. Cellular uptake of the NOTA-, DOTA-, and DTPA-repebodies was over 4-fold higher in H1650 cells than in SW620 cells at 1 h. The 3 repebodies had accumulated specifically in H1650 tumor–bearing nude mice by 1 h after intravenous injection and were retained for over 24 h, as measured by the percentage injected dose per gram of tissue (%ID/g). Tumor uptake of all repebodies increased from 1 to 6 h (at 1 h, 6.28, 8.46, and 6.91 %ID/g for NOTA-, DOTA-, and DTPA-repebody, respectively; at 6 h, 9.4, 8.28, and 10.1 %ID/g, respectively). H1650 tumors were clearly visible after injection of each repebody, with high tumor-to-background ratios (at 1 h, 3.43, 4.89, and 2.38 for NOTA-, DOTA-, and DTPA-repebody, respectively; at 6 h, 3.05, 4.36, and 2.08; at 24 h, 3.81, 4.58, and 2.86). **Conclusion:** The 3 ^{64}Cu-repebody complexes demonstrated specific and rapid uptake in EGFR-expressing tumors within 1 h and may have potential as novel EGFR imaging agents for PET.

Key Words: repebody; positron emission tomography; molecular imaging; ^{64}Cu labeling; EGFR

J Nucl Med 2018; 59:340–346
DOI: 10.2967/jnumed.117.197020

Cancer is a leading cause of human morbidity and mortality worldwide (*1*). Overexpression of genes that regulate proliferation, cell survival, metastasis, and angiogenesis has an important role in the development of cancer. One such gene, the epidermal growth factor receptor (*EGFR*, also known as erbB1 and HER1), has been implicated in the development of a wide range of tumors (*2*). EGFR is a member of the erbB (avian erythroblastosis oncogene B) family of receptor tyrosine kinases, which includes HER2/*neu* (erbB2), HER3 (erbB3), and HER4 (erbB4) (*3,4*). EGFR has been a target of considerable interest for cancer diagnosis and therapy because it is expressed at a high level in head and neck, breast, bladder, prostate, colorectal, kidney, lung, and brain cancer (*5–9*). However, the EGFR expression level is determined at biopsy, which is invasive and does not allow repeated measurements of EGFR expression (*10*).

To address this unmet clinical need, radiolabeled antibodies for PET imaging were developed to enable noninvasive, repeatable assessment of EGFR expression (*11–13*). These studies allowed visualization of tumoral EGFR expression in humans and mice. However, antibody-based imaging agents have technical limitations, such as a long residence time in the circulation and a slow penetration rate into the tumor, that result in a low tumor-to-blood ratio, translating into low contrast and, therefore, low-sensitivity imaging (*10*).

Through modular engineering approaches, a novel, nonantibody protein scaffold called a repebody, which comprises leucine-rich repeat modules, has been developed (*14–18*). Repebodies can be easily developed as high-affinity protein binders against a variety of epitopes through phage display and modular engineering, and this platform offers some advantages over immunoglobulin antibodies or artificial protein binders in terms of binding affinity, ease of engineering, and specificity. In this study, instead of using a monoclonal antibody as the protein binder, we used a repebody with high affinity for EGFR. A synthetic repebody library was constructed for a phase display, and a

Received Jun. 11, 2017; revision accepted Aug. 24, 2017.
For correspondence or reprints contact either of the following:
Jung-Joon Min, Department of Nuclear Medicine, Chonnam National University Medical School, 264, Seoyang-ro, Hwasun-eup, Hwasun-gun, Jeollanam-do, 58128, Republic of Korea.
E-mail: jjmin@jnu.ac.kr
Dong-Yeon Kim, Department of Nuclear Medicine, Chonnam National University Hwasun Hospital 322, Seoyang-ro, Hwasun-eup, Hwasun-gun, Jeollanam-do, 58128, Republic of Korea.
E-mail: blueburr@gmail.com
*Contributed equally to this work.
Published online Sep. 15, 2017.

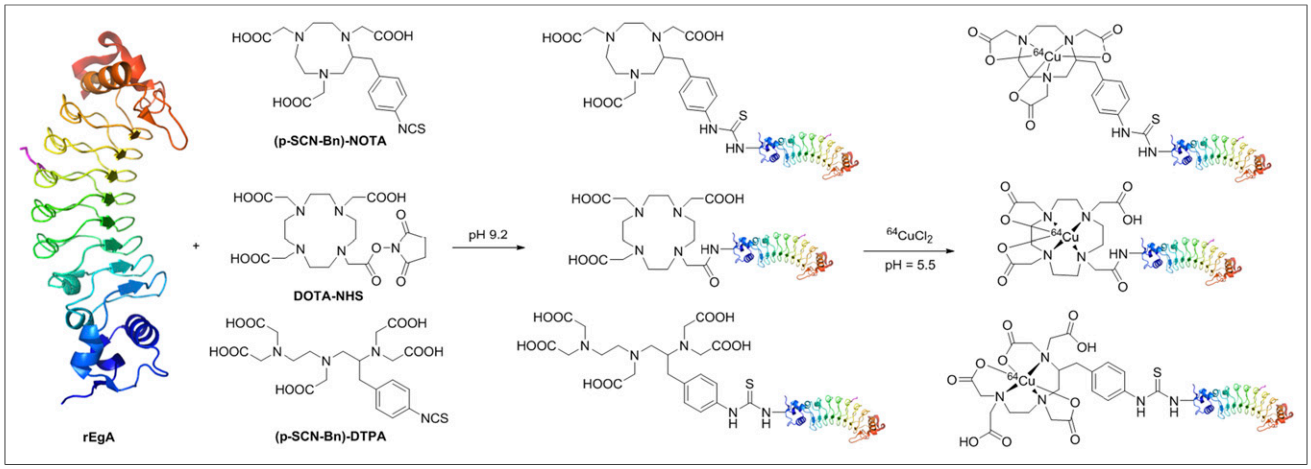

FIGURE 1. Synthesis scheme of NOTA-, DOTA-, and DTPA-conjugated rEgA and radiolabeling. NHS = *N*-hydroxysuccinimide.

repebody that could target the human soluble EGFR ectodomain was selected. This repebody (rEgA) has a nanomolar affinity (dissociation constant, 9.18 nM) (*14*).

Herein, we report the synthesis and characterization of 3 ^{64}Cu-labeled rEgA complexes (rEgA with NOTA, DOTA, and DTPA) for noninvasive and repeated PET assessment of EGFR expression in tumors. Biologic studies, such as cellular uptake assays, biodistribution studies, and small-animal PET imaging, were performed, and the radiolabeled repebodies were compared to identify the best candidate for an imaging tool for companion diagnosis of EGFR expression.

MATERIALS AND METHODS

Repebody Conjugation with Bifunctional Chelators (BFCs) and Radiolabeling

rEgA was incubated at a 5:1 molar ratio with 2-(*p*-isothiocyanatobenzyl)-1,4,7-triazacyclononane-*N*,*N*′,*N*,″-triacetic acid trihydrochloride ([*p*-SCN-Bn]-NOTA), 2,2′,2″-(10-(2-(2,5-dioxopyrrolidin-1-yloxy)-2-oxoethyl)-1,4,7,10-tetraazacyclododecane-1,4,7-triyl) triacetic acid (DOTA-*N*-hydroxysuccinimide ester), or 1-(*p*-isothiocyanatobenzyl) diethylenetriamine pentaacetic acid trihydrochloride ([*p*-SCN-Bn]-DTPA) in 1.0 M $NaHCO_3$ buffer (pH 9.2) for 24 h. The resulting products (NOTA-, DOTA-, and DTPA-rEgA) were purified using a disposable PD MiniTrap G-10 desalting column (GE Healthcare). All compounds were analyzed by MALDI-TOF mass spectroscopy to confirm their identities. $^{64}CuCl_2$ was produced at the Korea Institute of Radiologic and Medical Sciences by 50 MeV cyclotron irradiation using a previously reported method (*19*). ^{64}Cu was complexed with NOTA-, DOTA-, and DTPA-rEgA in 0.1 M NH_4OAc buffer (pH 5.5) at 40°C for 1 h, and then ^{64}Cu-rEgA variants were purified using G-10 columns. Radiochemical purity was determined by high-performance liquid chromatography with analytic size-exclusion chromatography (mobile phase starting from 70% solvent A [0.1% trifluoroacetic acid in water] and 30% solvent B [0.1% trifluoroacetic acid in acetonitrile] to 30% solvent A and 70% solvent B for 30 min; retention time: 12.1 min).

BFC-to-rEgA Ratio, Stability Assays, and Enzyme-Linked Immunosorbent Assay

The number of chelator groups per rEgA molecule was calculated as previously reported (*20*). In vitro and in vivo stability tests and enzyme-linked immunosorbent assays were performed as previously described (*14*).

Cell Lines, Culture Conditions, and Cellular Uptake Studies

Cellular uptake studies were performed to determine whether the addition of the various chelators to the rEgA would alter its specificity. Human non–small cell lung carcinoma (H1650) and human colorectal carcinoma (SW620) cell lines were obtained from the American Type Culture Collection. They were cultured in high-glucose RPMI medium. H1650 and SW620 cells (1×10^6) were plated in 12-well plates and incubated at 37°C for 1, 2, or 6 h with 0.74 MBq of ^{64}Cu-rEgA variants. The wells were washed 3 times with phosphate-buffered saline and harvested, and the cell-associated radioactivity was determined on a γ-counter. Data are expressed as the accumulation ratio (%) ± SD per 10^6 cells, which was calculated by dividing the radioactivity in the pellet by the radioactivity in the supernatant and pellet combined.

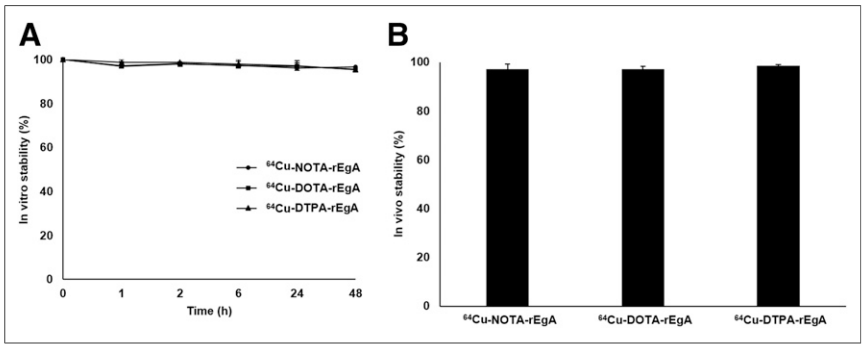

FIGURE 2. In vitro serum stability (A) and in vivo stability (B) of ^{64}Cu-labeled NOTA-, DOTA-, and DTPA-rEgA. In vitro and in vivo stability is expressed as mean ± SD.

Small-Animal PET Imaging of ^{64}Cu-rEgA Variants

Animal care, experiments, and euthanasia were performed in accordance with protocols approved by the Chonnam National University Animal Research Committee and the *Guide for the Care and Use of Laboratory Animals* (*21*). Male nude mice (5–6 wk old) were inoculated with H1650 or SW620 cells (10^6) subcutaneously in the right shoulder and were used for biodistribution, EGFR

targeting, pharmacokinetic, and small-animal PET studies when the tumors reached 150–200 mm^3 (~21 d). The biodistribution in various organs was assessed 1, 6, and 24 h after injection of 7.4 MBq of each ^{64}Cu-labeled rEgA radiotracer (n = 9 mice/group) into the tail veins of the mice, and images were acquired over a period of 10 min at 1, 6, and 24 h after injection (Inveon small-animal PET scanner; Siemens).

RESULTS

^{64}Cu Radiolabeling and Stability Assay

The scheme for the conjugation of rEgA with BFCs and ^{64}Cu labeling is shown in Figure 1. Conjugation of the BFCs through the *N*-hydroxysuccinimide ester or *p*-SCN-Bn linker proved highly amenable to the aqueous conditions required for solubilizing the rEgA. The results of MALDI-TOF mass spectroscopy are presented in Supplemental Figures 1–4 (supplemental materials are available at http://jnm.snmjournals.org). The overall decay-corrected radiochemical yield was approximately 70%–80%. Identification of the radioproduct through comparison of the collected high-performance liquid chromatography fraction with rEgA labeled with nonradioactive copper is shown in Supplemental Figures 5–7.

When the ^{64}Cu-rEgA variants were incubated in human serum at 37°C for 48 h, the amount remaining (R_f, 0.05–0.1) was greater than 95%, indicating a relatively high in vitro stability (Fig. 2A). Furthermore, no metabolites were detected in the serum of mice 6 h after intravenous injection of ^{64}Cu-rEgA variants (^{64}Cu-NOTA-rEgA: 97.12 ± 2.16; ^{64}Cu-DOTA-rEgA: 97.05 ± 1.22; ^{64}Cu-DTPA-rEgA: 98.45 ± 0.51 [n = 9]) (Fig. 2B).

Optimized BFC Number and Cellular Uptake

To optimize EGFR affinity and biocompatibility, various ratios of (*p*-SCN-Bn)-NOTA to rEgA were used in the conjugation reaction, ranging from 0.2:1 stoichiometry to 50:1. When the 0.2:1 equivalent of NOTA was used, the average number of NOTA groups per rEgA was 0.75 ± 0.18, excluding nonconjugated rEgA. The average numbers of NOTA groups after conjugation with the 1:1, 10:1, and 50:1 ratios were 0.58 ± 0.38, 4.97 ± 0.21, and 12.1 ± 2.31, respectively. Subsequently, rEgA with various numbers of NOTA groups were radiolabeled and used in cellular uptake assays in the H1650 cell line (EGFR-positive) (*22,23*). The highest accumulation in the H1650 cell line after 6 h of treatment (51.84% ± 6.01%) was achieved when rEgA was conjugated with (*p*-SCN-Bn)-NOTA at the 0.2 equivalent (Supplemental Fig. 8). Therefore, we adopted the 0.2 ratio of BFC for chelation of rEgA, and we prepared ^{64}Cu-NOTA-rEgA, ^{64}Cu-DOTA-rEgA (DOTA groups per rEgA: 0.66 ± 0.15), and ^{64}Cu-DTPA-rEgA (DTPA groups per rEgA: 0.69 ± 0.19) for in vitro and in vivo application. Furthermore, enzyme-linked immunosorbent assay revealed that the binding affinity of each of the 3 types of ^{nat}Cu-rEgA for the EGFR was similar to that of native rEgA (Supplemental Fig. 9).

Cellular uptake values for ^{64}Cu-rEgA in H1650 cells and SW620 cells (EGFR-negative) (*24,25*) over incubation periods of 1, 2, and 6 h are shown in Figure 3. Importantly, specific accumulation was observed with the ^{64}Cu-labeled rEgA conjugated to each chelator. The uptake of ^{64}Cu-labeled NOTA-, DOTA-, and DTPA-rEgA increased from 5.21% ± 0.10%, 15.18% ± 1.97%, and 19.50% ± 7.69%, respectively, at 1 h to 50.82% ± 4.23%, 45.76% ± 1.08%, and 59.34% ± 8.17%, respectively, at 6 h. Furthermore, the uptake of each ^{64}Cu-rEgA was more than 9-fold higher in H1650 cells than in SW620 cells at 6 h ($P < 0.05$). Specifically, the uptake of ^{64}Cu-NOTA-rEgA was over 14-fold higher in H1650 cells than in SW620 cells (50.82% ± 4.23% vs. 3.61% ± 0.50%, $P < 0.05$). Overall, these results suggest that the specificity of the rEgA for EGFR was well maintained after chelator-based radiolabeling.

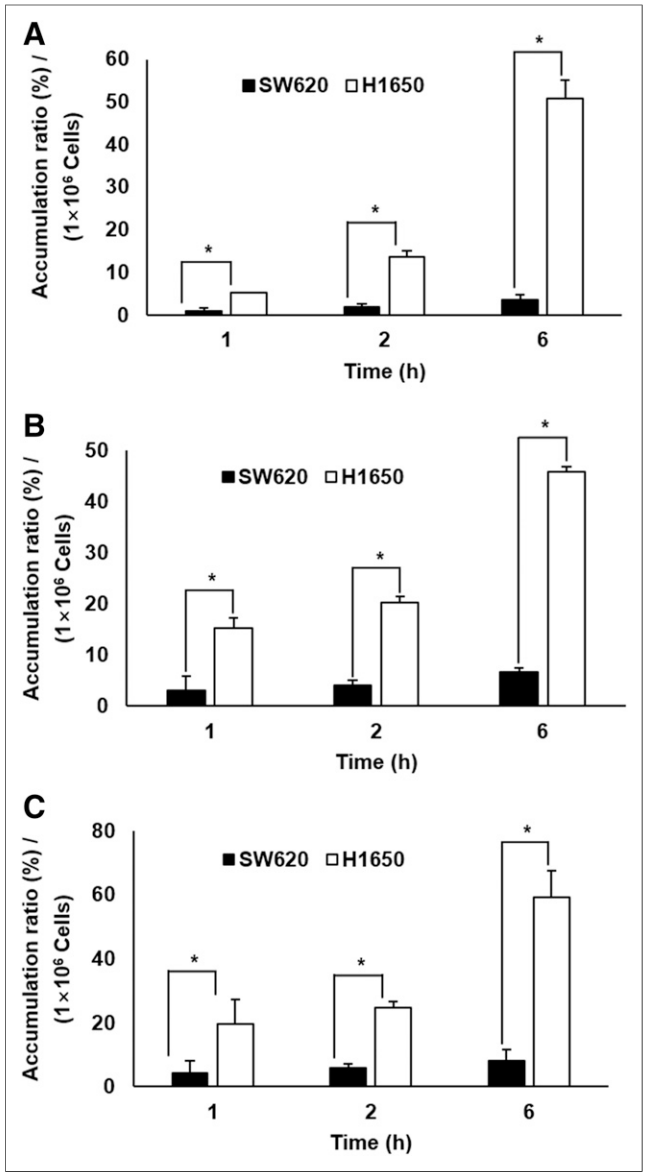

FIGURE 3. Cellular uptake of ^{64}Cu-NOTA-rEgA (A), ^{64}Cu-DOTA-rEgA (B), and ^{64}Cu-DTPA-rEgA (C) in SW620 and H1650 cells. All values are expressed as mean ± SD per 10^6 cells. *$P < 0.05$ (Mann–Whitney *U* test).

Biodistribution Studies and Small-Animal PET Imaging

The biodistribution of the 3 types of ^{64}Cu-rEgA is shown in Table 1. All exhibited rapid, high EGFR binding and prolonged tumor retention. The tumor uptake of ^{64}Cu-labeled NOTA-, DOTA-, and DTPA-rEgA (expressed as the percentage injected dose per gram of tissue [%ID/g]) was 8.89 ± 1.04, 7.58 ± 0.31, and 6.97 ± 1.50, respectively, 1 h after intravenous injection. All types of

TABLE 1
Biodistribution of ^{64}Cu-NOTA-rEgA, ^{64}Cu-DOTA-rEgA, and ^{64}Cu-DTPA-rEgA in H1650 Tumor–Bearing Nude Mice at 1, 6, and 24 Hours After Injection

	^{64}Cu-NOTA-rEgA			^{64}Cu-DOTA-rEgA			^{64}Cu-DTPA-rEgA		
Site	1 h	6 h	24 h	1 h	6 h	24 h	1 h	6 h	24 h
Blood	2.53 ± 0.22	2.98 ± 0.70	2.18 ± 0.05	2.15 ± 0.67	3.99 ± 1.95	2.17 ± 0.23	2.76 ± 1.16	2.24 ± 0.15	2.41 ± 0.28
Heart	5.09 ± 0.47	4.82 ± 0.47	4.53 ± 0.17	5.15 ± 0.37	4.15 ± 1.02	3.85 ± 0.68	5.56 ± 2.20	4.91 ± 0.65	4.05 ± 0.39
Lung	5.32 ± 1.81	6.13 ± 0.70	5.05 ± 0.77	4.60 ± 1.74	5.52 ± 2.72	5.13 ± 0.48	6.18 ± 3.80	7.42 ± 1.14	5.42 ± 1.02
Liver	13.71 ± 1.17	16.68 ± 1.38	16.58 ± 1.97	16.58 ± 0.92	19.45 ± 2.09	18.46 ± 2.65	25.24 ± 1.95	23.86 ± 1.80	22.44 ± 1.83
Spleen	3.60 ± 0.50	4.17 ± 0.17	3.92 ± 0.37	2.88 ± 0.14	4.48 ± 0.78	4.31 ± 0.46	5.67 ± 0.71	4.63 ± 0.74	4.63 ± 0.39
Stomach	2.67 ± 0.67	3.33 ± 1.15	4.01 ± 0.28	2.86 ± 0.84	2.73 ± 1.42	3.06 ± 1.22	7.02 ± 1.40	3.65 ± 2.05	4.16 ± 2.31
Intestine	11.41 ± 0.42	8.24 ± 0.97	5.64 ± 0.40	12.15 ± 1.14	7.63 ± 0.61	6.00 ± 1.56	15.18 ± 2.45	7.55 ± 0.30	6.14 ± 1.07
Kidney	20.33 ± 1.01	15.88 ± 2.36	15.21 ± 2.10	9.61 ± 0.25	10.88 ± 1.96	9.23 ± 0.69	17.41 ± 1.93	12.14 ± 0.13	12.85 ± 0.85
Pancreas	3.39 ± 0.24	3.65 ± 0.27	2.21 ± 0.18	2.68 ± 0.32	3.51 ± 0.95	3.06 ± 0.93	4.86 ± 0.51	3.25 ± 0.54	2.95 ± 0.48
Muscle	1.02 ± 0.17	0.89 ± 0.16	0.94 ± 0.15	0.79 ± 0.13	1.09 ± 0.14	1.30 ± 0.08	1.41 ± 0.28	0.98 ± 0.15	1.06 ± 0.12
Bone	1.04 ± 0.82	2.12 ± 0.58	1.63 ± 0.33	1.63 ± 0.43	1.74 ± 0.52	1.13 ± 0.34	1.58 ± 0.30	1.77 ± 0.46	1.82 ± 0.58
Brain	0.39 ± 0.06	0.51 ± 0.02	0.57 ± 0.04	0.30 ± 0.05	0.51 ± 0.05	0.63 ± 0.08	0.51 ± 0.12	0.52 ± 0.05	0.70 ± 0.05
Skin	4.23 ± 0.94	3.63 ± 0.43	2.38 ± 0.28	4.16 ± 1.76	4.55 ± 1.31	2.38 ± 0.19	4.10 ± 0.92	3.83 ± 0.31	2.77 ± 0.54
Tumor	8.89 ± 1.04	14.47 ± 1.68	9.97 ± 1.51	7.58 ± 0.31	14.33 ± 0.98	11.51 ± 1.35	6.97 ± 1.50	13.28 ± 2.22	11.61 ± 1.36

Data are expressed as %ID/g (n = 9 mice/group).

^{64}Cu-rEgA showed the highest tumor uptake at 6 h after injection (NOTA, 14.47 ± 1.68 %ID/g; DOTA, 14.33 ± 0.98 %ID/g; and DTPA, 13.28 ± 2.22). Even at 24 h after injection, the distribution of each type of ^{64}Cu-rEgA in the tumor was approximately 10.0%. High and rapid tumor uptake and prolonged retention coupled with rapid clearance and low nonspecific binding in normal organs resulted in high tumor-to-blood ratios (NOTA, 5.00 ± 0.77 %ID/g; DOTA, 4.25 ± 2.12 %ID/g; and DTPA, 6.01 ± 2.57 %ID/g at 6 h after injection) and high tumor–to–normal-muscle ratios (NOTA, 16.38 ± 1.79 %ID/g; DOTA, 13.35 ± 2.32 %ID/g; and DTPA, 13.95 ± 6.22 %ID/g at 6 h after injection) (Table 2). Furthermore, although hepatic uptake of DTPA was higher than that of NOTA and DOTA, there was no statistically significant difference among the 3 groups according to the results of the Mann–Whitney U test. Thus, hepatic uptake of ^{64}Cu-rEgA variants may be related to the biodistribution properties of rEgA (*26*).

Static PET images of H1650 or SW620 tumor–bearing mice at 1, 6, and 24 h after intravenous injection of the ^{64}Cu-rEgA are shown in Figure 4. The EGFR-expressing H1650 tumors could be clearly visualized at 1 h after injection, and tumor uptake was retained for 24 h. However, tumor uptake of ^{64}Cu-rEgA was the highest at 6 h after intravenous injection. To verify the specificity of the ^{64}Cu-rEgA for EGFR-expressing tumors, H1650 tumor–bearing mice were injected with cold rEgA (50 μM), and a small-animal PET study was performed with ^{64}Cu-NOTA-rEgA after 24 h. At 6 h, tumor uptake decreased from 100% without blocking to 39%, indicating the specificity of rEgA binding in vivo. Furthermore, free ^{64}Cu showed very low uptake in H1650 tumor–bearing mice, indicating that ^{64}Cu-rEgA has high specificity for the EGFR (Fig. 5). The quantified tumor, blood, and muscle uptake of the ^{64}Cu-rEgA are shown in Supplemental Figure 10, and the tumor-to-blood and -muscle ratios are compared in Figure 6. The 3 ^{64}Cu-rEgA cleared rapidly from the

TABLE 2
Comparison of Tumor-to-Blood and Tumor-to-Muscle Ratios at 1, 6, and 24 Hours After Administration of ^{64}Cu-NOTA-rEgA, ^{64}Cu-DOTA-rEgA, or ^{64}Cu-DTPA-rEgA to H1650 Tumor–Bearing Mice

Ratio	^{64}Cu-NOTA-rEgA	^{64}Cu-DOTA-rEgA	^{64}Cu-DTPA-rEgA
Tumor-to-blood			
1 h	3.50 ± 0.50	3.71 ± 0.95	2.57 ± 1.26
6 h	5.00 ± 0.77	4.25 ± 2.12	6.01 ± 2.57
24 h	4.58 ± 1.19	5.39 ± 1.11	4.76 ± 0.91
Tumor-to-muscle			
1 h	8.96 ± 2.72	9.74 ± 1.40	4.71 ± 1.72
6 h	16.38 ± 1.79	13.35 ± 2.32	13.95 ± 6.22
24 h	10.55 ± 1.14	8.90 ± 1.43	11.09 ± 3.36

blood, with less than 2 %ID/g remaining 1 h after injection. Small-animal PET images obtained with ^{64}Cu-labeled NOTA-, DOTA-, and DTPA-rEgA exhibited high tumor-to-blood (>5 at 6 h after injection) and tumor-to-muscle (>10 at 6 h after injection) ratios, as was consistent with the biodistribution results.

DISCUSSION

In this study, we generated 3 versions of ^{64}Cu-rEgA, which is a small (28.3 kDa) protein scaffold with high affinity and rapid penetration, to determine their utility as PET imaging agents for EGFR-expressing tumors. These molecules were found to be appropriate for the quantification of EGFR expression using PET. Furthermore, the present strategy can be widely applied to target different receptors for the detection of other cancers. Finally, as a molecular probe, the repebody scaffold has advantages over other formats because it is easy to engineer and highly stable over a wide range of pH and temperature values (*18*).

To synthesize PET molecular probes with rEgA, we chose ^{64}Cu because of its favorable decay characteristics (half-life, 12.7 h; β^+, 7.8%; β^-, 38.4%). ^{64}Cu was produced with a high yield and high specificity by the ^{64}Ni(p,n)^{64}Cu nuclear reaction using an MC50 cyclotron (Korea Institute of Radiologic and Medical Sciences). The rEgA was then ^{64}Cu-labeled through BFCs (NOTA, DOTA, and DTPA). Furthermore, the longer half-life of ^{64}Cu among positron emitters allows for imaging at later time points than ^{18}F (half-life, 109.7 min) and is more appropriate for imaging of protein binders (*27*). Two conjugation strategies (DOTA via the *N*-hydroxysuccinimide ester; NOTA and DTPA via the *p*-SCN-Bn linker group) were used, and the BFC-conjugated rEgA variants were efficiently radiolabeled with ^{64}Cu.

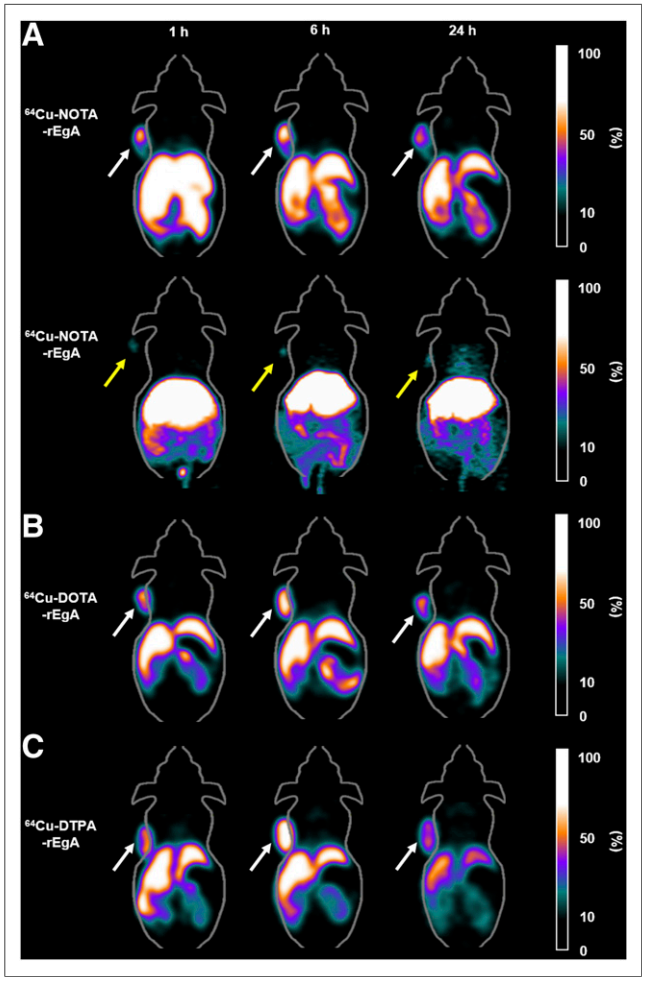

FIGURE 4. Coronal small-animal PET images of nude mice bearing H1650 (white arrows) or SW620 (yellow arrows) tumors at 1, 6, and 24 h after tail veil injection of ^{64}Cu-labeled NOTA-, DOTA-, or DTPA-rEgA (each at 7.4 MBq).

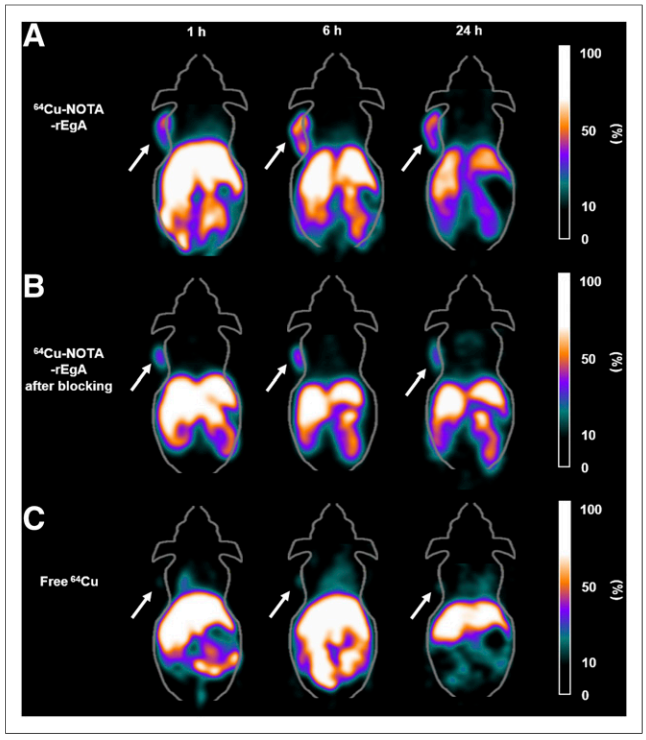

FIGURE 5. Coronal small-animal PET images of H1650 tumor–bearing nude mice (arrows) that were pretreated with phosphate-buffered saline (A) or 50 μM cold rEgA (B) 24 h before ^{64}Cu-NOTA-rEgA administration and coronal small-animal PET images of free ^{64}Cu in H1650 tumor–bearing nude mice. Images at 1, 6, and 24 h are shown.

Our cellular and animal experiments indicate that the rEgA is a potential molecular binder for the development of imaging probes to evaluate the presence and quantity of targets in tumor tissue. The cellular uptake study demonstrated that the specificity of the rEgA was not influenced by chelation with NOTA, DOTA, or DTPA. In vivo biodistribution studies showed a rapid accumulation of activity in the tumor, with stable retention for at least 24 h. Low uptake in blood and normal muscle resulted in high tumor-to-blood and tumor-to-muscle ratios. The biodistribution results were confirmed by small-animal PET imaging. EGFR specificity was also confirmed by a blocking study using nonlabeled rEgA. Although the biodistribution results showed a trend similar to small-animal PET data, the absolute values for tissue uptake obtained in the biodistribution study were higher. This discrepancy might have resulted from the way organ weight is calculated in small-animal PET. Although, in the ex vivo biodistribution studies, the weight of each organ was precisely measured using an electric balance, tissue weight was estimated in small-animal PET from the average weight of a single voxel, which is calculated from the whole-body weight divided by the total activity of voxels.

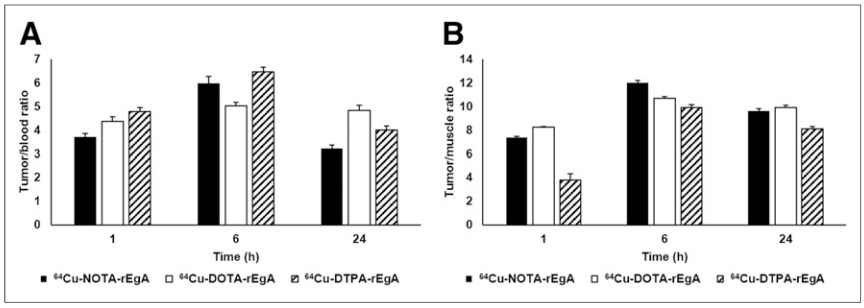

FIGURE 6. Comparison of tumor-to-blood (A) and tumor-to-muscle (B) ratios among ^{64}Cu-NOTA-rEgA, ^{64}Cu-DOTA-rEgA, and ^{64}Cu-DTPA-rEgA.

Because whole-body weight includes heavy components such as bone in addition to soft tissue such as tumor, tissue weight can be overestimated in PET imaging, potentially explaining why the %ID/g of PET imaging was lower than that of the ex vivo biodistribution study.

Development of imaging probes for visualization of EGFR expression has been reported, including a ^{111}In-labeled murine antibody (clone 225), ^{64}Cu-labeled peptides, and a ^{64}Cu-labeled chimeric cetuximab molecule for SPECT or PET imaging (*28–31*). Furthermore, in terms of in vivo performance, cetuximab variants labeled with ^{89}Zr (78.41 h) or ^{177}Lu (6.65 d) have a longer physical half-life than the ^{64}Cu-labeled molecule (*28,32,33*). However, EGFR expression with these radiolabeled antibodies could not be visualized in various solid tumors until after 24 h, because of low clearance and tissue penetration. In the present studies, EGFR expression could be visualized 1 h after injection of ^{64}Cu-rEgA, suggesting that radionuclides with short half-lives, such as ^{18}F (109.8 min) and ^{68}Ga (68 min), might also be useful as rEgA conjugates.

CONCLUSION

The 3 ^{64}Cu-rEgA variants were synthesized easily under mild conditions, and their in vitro and in vivo characteristics were evaluated. The rapid and prolonged retention of ^{64}Cu-rEgA in the tumor but not the blood or muscle suggests that these molecules can be used as imaging agents to obtain high-contrast PET images of EGFR expression at tumor sites shortly after injection. Our results demonstrate that the specific nature of the rEgA for targeting was not influenced by the various BFCs. The favorable in vivo kinetics and specific tumor uptake of ^{64}Cu-rEgA warrant its further investigation for imaging of EGFR-positive tumors. Therefore, rEgA has potential as a novel scaffold for the development of imaging agents for companion diagnosis.

DISCLOSURE

This study was supported by a grant from the Bio and Medical Technology Development Program of the National Research Foundation (NRF) of Korea (NRF-2014M3A9B5073747) and by the Pioneer Research Center Program of the NRF of Korea (2015M3C1A3056410), funded by the Ministry of Science, Communications Technology (ICT), and Future Planning. Hyeon Sik Kim was supported by the Basic Science Research Program through the NRF of Korea, funded by the Ministry of Education (NRF-2016R1D1A3B01006631), and Hee-Seung Bom was supported by the Basic Science Research Program through the NRF of Korea, funded by the Ministry of Education (NRF-2016R1D1A3B01006631). Dong-Yeon Kim was supported by the Basic Science Research Program through the NRF of Korea, funded by the Ministry of Education (17R1D1A1B03029055). No other potential conflict of interest relevant to this article was reported.

ACKNOWLEDGMENT

We thank Gyeongmin Kim for his excellent research assistance.

REFERENCES

1. Simon N, FitzGerald D. Immunotoxin therapies for the treatment of epidermal growth factor receptor-dependent cancers. *Toxins (Basel).* 2016;8:137.
2. Chong CR, Janne PA. The quest to overcome resistance to EGFR-targeted therapies in cancer. *Nat Med.* 2013;19:1389–1400.
3. Ono M, Kuwano M. Molecular mechanisms of epidermal growth factor receptor (EGFR) activation and response to gefitinib and other EGFR-targeting drugs. *Clin Cancer Res.* 2006;12:7242–7251.
4. Scaltriti M, Baselga J. The epidermal growth factor receptor pathway: a model for targeted therapy. *Clin Cancer Res.* 2006;12:5268–5272.
5. Nicholson RI, Gee JM, Harper ME. EGFR and cancer prognosis. *Eur J Cancer.* 2001;37(suppl):S9–S15.
6. Schlomm T, Kirstein P, Iwers L, et al. Clinical significance of epidermal growth factor receptor protein overexpression and gene copy number gains in prostate cancer. *Clin Cancer Res.* 2007;13:6579–6584.
7. Parra HS, Cavina R, Latteri F, et al. Analysis of epidermal growth factor receptor expression as a predictive factor for response to gefitinib ('Iressa', ZD1839) in non-small-cell lung cancer. *Br J Cancer.* 2004;91:208–212.
8. Zlobec I, Vuong T, Hayashi S, et al. A simple and reproducible scoring system for EGFR in colorectal cancer: application to prognosis and prediction of response to preoperative brachytherapy. *Br J Cancer.* 2007;96:793–800.
9. Nieto Y, Nawaz F, Jones RB, Shpall EJ, Nawaz S. Prognostic significance of overexpression and phosphorylation of epidermal growth factor receptor (EGFR) and the presence of truncated EGFRvIII in locoregionally advanced breast cancer. *J Clin Oncol.* 2007;25:4405–4413.
10. Garousi J, Andersson KG, Mitran B, et al. PET imaging of epidermal growth factor receptor expression in tumours using ^{89}Zr-labelled ZEGFR:2377 affibody molecules. *Int J Oncol.* 2016;48:1325–1332.
11. Menke-van der Houven van Oordt CW, Gootjes EC, Huisman MC, et al. ^{89}Zr-cetuximab PET imaging in patients with advanced colorectal cancer. *Oncotarget.* 2015;6:30384–30393.
12. Nayak TK, Regino CA, Wong KJ, et al. PET imaging of HER1-expressing xenografts in mice with ^{86}Y-CHX-A''-DTPA-cetuximab. *Eur J Nucl Med Mol Imaging.* 2010;37:1368–1376.
13. Eiblmaier M, Meyer LA, Watson MA, Fracasso PM, Pike LJ, Anderson CJ. Correlating EGFR expression with receptor-binding properties and internalization of ^{64}Cu-DOTA-cetuximab in 5 cervical cancer cell lines. *J Nucl Med.* 2008;49:1472–1479.
14. Yun M, Kim DY, Lee JJ, et al. A high-affinity repebody for molecular imaging of EGFR-expressing malignant tumors. *Theranostics.* 2017;7:2620–2633.
15. Hwang DE, Ryou JH, Oh JR, Han JW, Park TK, Kim HS. Anti-human VEGF repebody effectively suppresses choroidal neovascularization and vascular leakage. *PLoS One.* 2016;11:e0152522.
16. Lee JJ, Choi HJ, Yun M, et al. Enzymatic prenylation and oxime ligation for the synthesis of stable and homogeneous protein-drug conjugates for targeted therapy. *Angew Chem Int Ed Engl.* 2015;54:12020–12024.
17. Lee JJ, Kim HJ, Yang C-S, et al. A high-affinity protein binder that blocks the IL-6/STAT3 signaling pathway effectively suppresses non–small cell lung cancer. *Mol Ther.* 2014;22:1254–1265.
18. Lee SC, Park K, Han J, et al. Design of a binding scaffold based on variable lymphocyte receptors of jawless vertebrates by module engineering. *Proc Natl Acad Sci USA.* 2012;109:3299–3304.
19. Kim JY, Park H, Lee JC, et al. A simple Cu-64 production and its application of Cu-64 ATSM. *Appl Radiat Isot.* 2009;67:1190–1194.
20. Cai W, Chen K, Mohamedali KA, et al. PET of vascular endothelial growth factor receptor expression. *J Nucl Med.* 2006;47:2048–2056.

21. *Guide for the Care and Use of Laboratory Animals.* 8th ed. Washington, DC: National Academy Press; 2011.
22. Yang CH, Chou HC, Fu YN, et al. EGFR over-expression in non-small cell lung cancers harboring EGFR mutations is associated with marked down-regulation of CD82. *Biochim Biophys Acta.* 2015;1852:1540–1549.
23. Cross DA, Ashton SE, Ghiorghiu S, et al. AZD9291, an irreversible EGFR TKI, overcomes T790M-mediated resistance to EGFR inhibitors in lung cancer. *Cancer Discov.* 2014;4:1046–1061.
24. Petrulli JR, Sullivan JM, Zheng MQ, et al. Quantitative analysis of [^{11}C]-erlotinib PET demonstrates specific binding for activating mutations of the EGFR kinase domain. *Neoplasia.* 2013;15:1347–1353.
25. Yang JL, Qu XJ, Russell PJ, Goldstein D. Regulation of epidermal growth factor receptor in human colon cancer cell lines by interferon alpha. *Gut.* 2004;53:123–129.
26. Cooper MS, Ma MT, Sunassee K, et al. Comparison of ^{64}Cu-complexing bifunctional chelators for radioimmunoconjugation: labeling efficiency, specific activity, and in vitro/in vivo stability. *Bioconjug Chem.* 2012;23:1029–1039.
27. Liu Z, Li ZB, Cao Q, Liu S, Wang F, Chen X. Small-animal PET of tumors with ^{64}Cu-labeled RGD-bombesin heterodimer. *J Nucl Med.* 2009;50:1168–1177.
28. Song IH, Lee TS, Park YS, et al. Immuno-PET imaging and radioimmunotherapy of ^{64}Cu-/^{177}Lu-labeled anti-EGFR antibody in esophageal squamous cell carcinoma model. *J Nucl Med.* 2016;57:1105–1111.
29. Ping Li W, Meyer LA, Capretto DA, Sherman CD, Anderson CJ. Receptor-binding, biodistribution, and metabolism studies of ^{64}Cu-DOTA-cetuximab, a PET-imaging agent for epidermal growth-factor receptor-positive tumors. *Cancer Biother Radiopharm.* 2008;23:158–171.
30. Cai W, Chen K, He L, Cao Q, Koong A, Chen X. Quantitative PET of EGFR expression in xenograft-bearing mice using ^{64}Cu-labeled cetuximab, a chimeric anti-EGFR monoclonal antibody. *Eur J Nucl Med Mol Imaging.* 2007;34:850–858.
31. Wen X, Wu QP, Ke S, et al. Conjugation with ^{111}In-DTPA-poly(ethylene glycol) improves imaging of anti-EGF receptor antibody C225. *J Nucl Med.* 2001;42:1530–1537.
32. Liu Z, Ma T, Liu H, et al. ^{177}Lu-labeled antibodies for EGFR-targeted SPECT/CT imaging and radioimmunotherapy in a preclinical head and neck carcinoma model. *Mol Pharm.* 2014;11:800–807.
33. Aerts HJ, Dubois L, Perk L, et al. Disparity between in vivo EGFR expression and ^{89}Zr-labeled cetuximab uptake assessed with PET. *J Nucl Med.* 2009;50:123–131.

Errata

In the article "^{177}Lu-PSMA Radioligand Therapy for Prostate Cancer" by Fendler et al. (*J Nucl Med*. 2017;58:1196–1200), the "Indication" section incorrectly states that ^{177}Lu-PSMA RLT may be considered in patients with sufficient bone marrow reserve as defined by a white blood cell count *lower than* 3,000/μL and a platelet count *lower than* 75,000/μL. The correct levels are *higher than* 3,000/μL and *higher than* 75,000/μL, respectively. We regret the error.

In the article "Tumor Uptake of ^{64}Cu-DOTA-Trastuzumab in Patients with Metastatic Breast Cancer" by Mortimer et al. (*J Nucl Med.* 2018;59:38–43), data in the HER2– column of Table 1 were left out because of a copyediting error. The corrected table appears below. We regret the error.

TABLE 1
Patient Demographics and Clinical Characteristics

Characteristic	HER2+ (n = 11)	HER2– (n = 7)
Median age (y)	59 y (age range, 35–75 y)	61 y (age range, 40–71 y)
Hormone receptor and HER2 status of recurrence		
ER and PR receptors		
ER- and/or PR-positive	6	3
ER-negative and PR-negative	5	4
HER2		
IHC1+		4
IHC2+	3	3
IHC3+	8	
Prior HER2-directed therapy		
Trastuzumab for metastasis	8 (79 d–36 mo)	
None	3	7
Sites of metastatic disease measured for SUV_{max}		
Bone	24	12
Lymph nodes	23	10
Liver	6	0
Lung	6	3
Other*	2	3
Breast/chest wall†	5	5
Tumor volume (cm^3)‡		
Mean	5.8	12.2
SE	0.9	2.7

*Pulmonary effusion (HER2+) or body wall outside breast region.
†Breast or chest wall adjacent to breast.
‡Volume within isocontour of ^{18}F-FDG tumor image approximately matching boundary of CT correlate.
HER2 = human epidermal growth factor receptor 2; ER= estrogen receptor; PR= progesterone receptor; IHC = immunohistochemistry; SE = standard error.